Sustainable Food Technology

Accepted Manuscript

This article can be cited before page numbers have been issued, to do this please use: R. Ranjan, C. Kant and P. Dhar, *Sustainable Food Technol.*, 2025, DOI: 10.1039/D5FB00355E.

ROYAL SOCIETY OF CHEMISTRY

Sustainability spotlight

Plastic packaging plays major role in environmental pollution and depletion of resources. This research introduces an innovative approach by transforming sugarcane bagasse, a plentiful agricultural byproduct, into biodegradable, flame-retardant, and mechanically strong cellulose phosphate-based food packaging films. The films fabricated through sustainable methods enhance the shelf-life of perishable food items, comply with safety regulations, and decompose within 56 days, providing an environmentally-friendly substitute for traditional petroleum-derived plastics. The analysis of life cycle indicates a reduced carbon footprint and minimal negative environmental effects. This study is in accordance with UN Sustainable Development Goals, specifically focusing on SDG 12 (Responsible Consumption and Production), SDG 13 (Climate Action), and SDG 9 (Industry, Innovation and Infrastructure), by advocating for circular economy principles and advancements in sustainable materials.

View Article Online
DOI: 10.1039/D5FB00355E

ARTICLE

Multifunctional cellulose phosphate-based food packaging films from biomass: Structure-functional relationship and environmental assessment studies

Received 00th January 20xx,
Accepted 00th January 20xx

DOI: 10.1039/x0xx00000x

Rahul Ranjan[a], Chandra Kant[b] and Prodyut Dhar[a†]

Sugarcane bagasse (SB), an agricultural biomass produced on a global scale, is generally subjected to improper disposal such as landfill dumping, open burning, or treated as waste. The present study aims to transform SB waste into value-added cellulose phosphate-based gels and packaging films through a green, scalable and sustainable route using agro-based chemicals. SB biomass was processed through delignification-cum-phosphorylation routes to produce gels of varying charge density (500 to 1130 mmol/kg) with a transition in colour from transparent to light yellow. The processed transparent films were flame-retardant and thermally stable due to the presence of phosphate groups, mechanically robust under both dry and wet conditions due to thermal–induced cross-linkings, as confirmed through FTIR and XPS studies. The life cycle assessment (LCA) studies for film production show reduced carbon footprint with improved environmental sustainability, biodegradability(~56 days) and migration values within standard limits, making it suitable for food packaging applications. The packaging of perishable milk products such as paneer using developed films resulted in extension of shelf-life by 14 days with no alterations in pH, peroxide values and without any growth of pathogenic bacteria. The present study overcomes challenges associated with traditional cellulose packaging and up-converts agro-biomass waste to value-added multifunctional films with promising packaging applications as a sustainable substitution to petroleum-based plastic packaging.

1. Introduction

Plastic packaging films have offered flexible and convenient solutions, which resulted in significant demand in a consumer-oriented world, but led to various health, environmental, and sustainability challenges. These issues have prompted increased demand for biopolymers and biodegradable polymers such as cellulose, pectin, gelatin, chitosan, starch, polylactic acid, and polyhydroxybutyrate-based packaging material as an environmentally-friendly substitute [1]. Sugarcane is a widely grown annual crop extensively utilised for sugar production and bioenergy applications. Sugarcane bagasse (SB) constitutes about~14-28% of the sugarcane plant, because of which it is generated in high-volume post-harvest, making it a widely available agricultural residue. SB primarily comprises cellulose, hemicellulose, and lignin, with cellulose being the most abundant component, accounting for 40% to 45% of bagasse fibres [2]. In recent years, cellulose from SB has been used for various applications such as thermal insulation, oil spill cleaning [3], heavy metals removal [4], sound absorbing material [5], packaging material [6], microbial fuel cell [7], biochar production, bioethanol [8], hydrogels [9], supercapacitor [10]. Over the years, this has been achieved through strategic chemical functionalisation of SB *via* amination [11], sulphonation [12], iodisation [13], TEMPO-oxidation [14], phosphorylation [15], *in-situ* modification using MoS_2 [16], graphene oxide [17], iron nanoparticles [4], TiO_2 nanoparticles [18], etc, converting the waste-to-value-added products for potential commercial applications.

In recent years, phosphorylation has attracted significant attention from the research community as a versatile functionalisation technique. This method involves chemically modifying cellulose by introducing anionic groups using various phosphorylating agents, such as phosphoric acid, di-ammonium hydrogen phosphate (DAHP), urea, phytic acid, ammonium dihydrogen phosphate, phosphorus acid, phosphorus pentoxide, and phosphorus oxychloride [19]. The interest in phosphorylation originates from its ability to tune the physicochemical and structural properties with charge content, along with-it imparting flame-retardancy, enhancing water absorption, and improving adsorption capacity. The oxidative phosphorylation of cellulose using urea and ammonium salts is a green route for modification. Additionally, urea facilitates cellulose swelling, aiding penetration of phosphorylating agents with a decrease in dissolution, thereby preventing its degradation [15]. In a recent study, Messa et al. produced phosphorylated SB-based porous structures through

[a] School of Biochemical Engineering, Indian Institute of Technology (BHU), Varanasi, Uttar Pradesh-221005, India
[b] Department of Chemical Engineering, Indian Institute of Technology (BHU), Varanasi, Uttar Pradesh-221005, India

spray-, oven-, and freeze-drying with improved thermal stability and tuneable charge content for potential fertiliser release [20]. Lu et al. developed a TEMPO-oxidised hydrogel using SB as a potential colorimetric sensor to monitor pH and CO_2 absorption in packaged chicken [14]. Gan et al. hydrolysed SB to produce phosphorylated cellulose nanocrystals using phosphoric acid, with tuneable morphology and crystallinity [21]. SB waste is extensively used for cellulose extraction or processed into micro/nanofibers for composite development; however, processing into flexible and transparent food packaging films has been seldom reported.

The present study utilised a green and sustainable method of functionalizing SB waste following delignification and phosphorylation routes to produce films for food packaging applications. The phosphorylation of SB biomass was carried out through solid-state curing at different time intervals (30-90 minutes), which led to variation in charge content of gels, ~500 to 1130 mmol/kg, with a transition in colour from transparent to light yellow. The gels with different charge contents were subsequently processed into films, and their effect on mechanical strength, thermal stability, and flame-retardant properties was evaluated in detail. SCBF films showed improved biodegradability, and LCA studies were carried out to determine the sustainability of the production process through evaluation of environmental impact parameters. The films sustained the aqueous environment without any disintegration, high water stability and migration values within permissible limits, making it suitable for food storage applications. The easily perishable milk products, such as paneer, were sealed in the developed films to evaluate their shelf-life in terms of rise in pH, peroxide values and growth of pathogenic bacteria under different conditions.

2. Materials and methods

The sugarcane bagasse (SB) utilised in this study was obtained from a juice vendor, Banaras Hindu University (BHU), Varanasi. Sodium acetate trihydrate (99% purity), urea (99.7% purity), glacial acetic acid, sodium chlorite (84% purity), and DAHP (97% purity) were purchased from Molychem Pvt. Ltd., India. The isooctane, violet red bile agar (VRBA), potato dextrose agar (PDA), xylose lysine deoxycholate (XLD) agar, polymyxin acriflavin lithium-chloride ceftazidime esculin mannitol (PALCAM) agar, de Man, Rogosa and Sharpe (MRS) agar, and Pseudomonas agar used in this study were obtained from Sisco Research Laboratory (India). All the experiments in this study were carried out using ultrapure water with a conductivity of 0.66 mΩ-cm obtained from a Direct-Q® 3UV unit (Merck Millipore, India).

2.1 Delignification and phosphorylation of bagasse

Delignifying solutions were prepared using sodium acetate trihydrate (5.4 wt.%), glacial acetic acid (2.4 v.%), and sodium chlorite (3 wt.%) dissolved in distilled water. The SB was washed, cut into 3-5 cm long pieces, and immersed in the delignifying solution. The delignification reaction was performed at 80°C for 14 hours in a hot air oven. After the delignification, SB was washed with distilled water 4-5 times to remove the salts, impurities, and air dried (hereafter named as DSB). The DSB was mixed with phosphorylating agent (6 wt.% urea and 1.5 wt.% DAHP) and incubated at 70°C for 3 hours. After the incubation, the solutions were evaporated at 105°C, followed by curing at 150°C for 30, 45, 60, 75 and 90 minutes. The cured DSBs were washed with distilled water (3-4 times) to remove unreacted urea and DAHP salts, which resulted in the formation of phosphorylated bagasse gel.

2.2 Production of films using phosphorylated bagasse gels

The phosphorylated bagasse gel obtained was homogenised in a grinder for 5 minutes to uniformly disintegrate any clumps and produce the gels. Subsequently, the gels were mixed with distilled water, and the prepared suspensions were poured into a petri dish with a diameter of 15 cm and dried at 60°C for 4 hours. The films produced from the gels after the 30,45,60,75, and 90-minute curing time were designated as SCBF-30, SCBF-45, SCBF-60, SCBF-75, and SCBF-90, respectively.

2.3. Analytical characterisation

2.3.1 Conductometric titration

The dried films (0.3 g) were dissolved in 100 ml of distilled water containing 10 ml of sodium chloride solution (0.01 M) to produce a suspension. The suspension's pH was lowered to 3 by adding hydrochloric acid (0.1M) to initiate the reaction. Sodium hydroxide (NaOH) solution (200 µl) was added to initiate the reaction, and conductivity was recorded (EUTECH-PC700, Singapore) after each 200 µl addition (Ait Benhamou et al., 2021). The measurement continued till the pH of the suspension increased to 11, and charge content (CC, millimole/kg) was calculated from equation (1).

$$CC = \frac{Molarity\ of\ NaOH\ (M) \times Volume\ of\ NaOH\ (L)}{wet\ of\ the\ dried\ gel\ (g)} \times 10^6$$

eq. (1)

2.3.2 Attenuated total reflection Fourier transformation infrared Spectroscopy (ATR-FTIR)

FTIR of the films and DSB were performed on Nicolet-iS5 (Thermo-fisher, US) equipped with diamond crystals in ATR mode. 64 scans were recorded for each sample with 4 cm^{-1} resolution in the range of 4000-650 cm^{-1}.

2.3.3 X-ray photoelectron microscopy (XPS)

XPS of SCBF-60 film was performed with Thermo Scientific K alpha XPS (U.S.A.). The analysis was performed in a vacuum with a 400

µm beam spot. The survey scans for elements C, O, and P were recorded over the binding energy range 0-1300 eV. The broad spectra for O, P and C were recorded at an applied voltage of 0.1 eV for 100 seconds and 85 seconds, respectively, and ten scans were recorded for each element.

2.3.4 X-ray diffraction (XRD)

The XRD analysis of the films and DSB were measured using a benchtop MiniFlex 600 XRD (Rigaku, Japan) with X-rays produced by a copper anticathode. The spectra were recorded in the 2-theta range of 5-70° at applied voltage (40 kV) and current (40 mA). The crystallinity index (CrI) of samples was calculated using equation 2.

$$CrI\ (\%) = \frac{Intensity\ at\ 22.2° - Intensity\ at\ 18.5°}{Intensity\ at\ 22.2°} \quad \text{eq. (2)}$$

2.3.5 Thermal stability

The thermal stability of SCBF films and DSB were studied with TGA-50 (Perkin Elmer, Asia-Pacific). The analysis was performed with 5 mg of samples in an inert environment (N_2 supply flow rate 100 mL/min) over the 25-700°C temperature range.

2.3.6 Water absorption capacity

The initial weight ($W_{initial}$) of dried films (2 cm × 2 cm) was measured and thereafter immersed in distilled water for 24 hours. The final weight of the films was taken after 24 hrs (W_{final}). The water absorption capacity (W_A) of the samples was calculated from equation 3.

$$W_A\,(\%) = \frac{W_{final} - W_{initial}}{W_{final}} \times 100 \quad \text{eq. (3)}$$

2.3.7 Mechanical property

The mechanical properties of films (8 cm × 2 cm) were measured using a texture analyser (Shimadzu, Japan) at a crosshead speed of 1 mm/min, equipped with a load cell of 500 N.

2.3.8 Flammability test

The flammability test of the films (2 cm × 6 cm) in triplicate was performed under the direct flame of a spirit lamp. The average burning rate was calculated in terms of the change in length of burnt film in units of seconds, and the residual weight generated after burning was reported.

2.3.9 Wettability

The contact angle of films was measured on a contact angle goniometer (Theta Lite, Biolin Scientific, Sweden) equipped with a telecentric optics camera with a 50 mm focus. The samples were attached to double-sided tape to fix onto glass slides, and experiments were conducted at 25 ± 2°C. A micropipette was used to dispense 5 µl of distilled water onto the surface of films, and the resulting contact angles were recorded at a rate of 51 frames per second and analysed using Oneattention software.

2.3.10 Migration study

The migration study of films (2.5 cm × 4 cm) was exposed to two food-grade simulants following the guidelines specified in EU regulation No. 10/2011: 10 mL of isooctane for 2 days at 20°C and 10 mL of 10% (v/v%) ethanol for 10 days at 40°C. After the incubation period, samples were retrieved, and simulant materials were subjected to evaporation at 100°C to determine the migrated residue. The residue was then carefully weighed on a Shimadzu analytical balance (ATX224, Japan, with an accuracy of 0.01 mg) to calculate the overall migration in micrograms per kilogram (µg/kg).

2.4 Packaging and evaluation of the shelf-life of paneer

A film of dimension 10 cm × 6 cm was used to pack paneer of dimension 2 cm × 1.5 cm. The corners or the edges of the films were joined using SCBF gel under hot pressing conditions (Temperature 80-90°C for 180 seconds). The packed samples were incubated at 4°C for 21 days. The paneer kept outside without packaging at 4°C was taken as a control in the study. The changes in physico-chemical properties of paneer, such as pH, peroxide value and microbial load with and without packaging were evaluated following an earlier reported study (Umaraw et al., 2022). The pH measurement involved preparing a consistent paste by mixing 10 grams of paneer with 10 mL of distilled water. The peroxide value of the paneer was evaluated from a modified protocol reported by Hosseini et al. (Hosseini et al., 2023). Initially, 10 grams of paneer were mixed with a mixture of methanol and chloroform in a 3:2 ratio. This mixture was allowed to stand for 40 minutes, then filtered using a Whatman filter paper, followed by solvent evaporation using a rotary evaporator. Subsequently, 0.1 grams of the extracted residues were blended with a mixture of chloroform and acetic acid in a 3:2 ratio. After thorough mixing, 1 ml of potassium iodide was introduced into the mixture, which was then kept in the dark for 20 minutes. In addition, the mixture was subjected to titration using 0.02 M thiosulfate until the solution's colour changed to yellow. A 1.5 wt.% starch solution was introduced, and the titration was continued until the solution became colourless. The paneer's peroxide values (PV) were then determined using equation (4).

$$PV = M \times \frac{V - V_0}{2W} \times 100 \quad \text{eq. (4)}$$

where M represents the molarity of sodium thiosulfate (measured in mol/L), V indicates the volume of sodium thiosulfate used during

titration (measured in mL), V_O denotes the volume of sodium thiosulfate utilised for titration of the blank sample (measured in mL), and W represents the weight of the sample in grams.

Furthermore, microbiological tests of the packaged paneer were performed to evaluate the growth of pathogenic microorganisms over the incubation period; for the yeast and coliform, PDA and VRBA agar were used, respectively. To evaluate the growth of Pseudomonas, Salmonella and Listeria monocytogenes, Pseudomonas agar, XLD agar and PALCAM agar were used, respectively. Aseptically, 1 gram of paneer was homogenised in sterile distilled water (10 mL) in a laminar hood, and thereafter, 100 µL of the homogenised sample was placed onto respective agar plates. The plates for the PDA agar were incubated at 25°C, and the rest were incubated at 37°C for 24 hours. The resulting colonies were counted and expressed as log CFU/g (Xia et al., 2023).

2.5 Biodegradation of films

To evaluate the biodegradability, films were placed in garden soil, specifically at a depth of approximately 6 cm below the soil's surface. The film's biodegradation was determined by calculating the percentage (%) of biodegradation based on the weight loss between the film's initial and final weight at different time intervals using the equation.

$$Biodegradation\ (\%) = \frac{W_{IS} - W_{FS}}{W_{IS}} \times 100 \qquad \text{eq. (5)}$$

where W_{IS} is the weight of the film at the initial stage, and W_{FS} is the weight of the film at the final stage.

2.6 Life cycle assessment (LCA) of films

LCA is a widely accepted international standard, specifically ISO 14040 and ISO 14044, for quantifying relevant emissions and their corresponding environmental and health impacts from product or process development. The main objective of this study is to evaluate the cradle-to-gate analysis of SCBF film production from delignification of SB, followed by phosphorylation, homogenisation, casting and drying as main production routes. This study aims to identify critical aspects within the manufacturing process, particularly those that significantly impact the product's overall ecological impact. This information could be of great value during the transition from laboratory-scale to large-scale production to minimise the product's environmental impact.

The production of 4.7 g of SCBF film is considered a functional unit in this study. **Figure S5** represents the flow diagram for the production of SCBF film, and a list of assumptions is mentioned in Table S1. The analysis was performed using GaBi software (version 9.2.1.68), and primary sources utilised for input data were the Ecoinvent and GaBi databases. In laboratory-scale operations, the predominant energy source is primarily obtained from electricity generated by hard coal. The mid-point results were normalised to identify the significant dominant environmental categories using GaBi software.

A sensitivity analysis was conducted to investigate the effects of variations in critical factors on the environmental impacts within the most prominent categories. The key factors identified in the laboratory-scale production of SCBF films were electricity consumption, delignification, and phosphorylation. A sensitivity analysis was performed by adjusting the critical parameters with a positive variation of 10% and a negative variation of 8%. The present analysis primarily concentrated on the environmentally significant impact categories associated with the delignification and phosphorylation technique.

2.7 Water Vapour Permeability

The water vapour transmission rate (WVTR) of the SCBF (30-90) samples was assessed using the gravimetric cup method according to ASTM E96 standards [22]. Circular film specimens, measuring 9 cm in diameter, were securely mounted to aluminium test cups, providing an exposed permeation area of 25 cm². The cups contained 10 g of anhydrous silica gel to achieve an internal relative humidity (RH) of roughly 0%. The prepared cups were subsequently placed in a controlled desiccator environment maintained at 25 °C and 75% relative humidity, utilizing a saturated sodium chloride (NaCl) solution. Mass variations in the cups were measured gravimetrically at 2-hour intervals over 24 hours, utilizing an analytical balance with a resolution of 0.0001 g. All measurements were performed in triplicate to ensure reproducibility. WVTR and water vapour permeability (WVP) were calculated using equations 6 and 7.

$$WVTR = \frac{\Delta W}{A\,(m^2) \times time\,(h)} \qquad \text{eq. (6)}$$

$$WVP = \frac{\Delta W \times film\ thickness\,(mm)}{A\,(m^2) \times time\,(s) \times \Delta P\,(Pa)} \qquad \text{eq. (7)}$$

where, ΔW is the change in the weight of the aluminium cup utilized for the test, A is the exposed area of the film mounted on the cup, and ΔP water vapour pressure across the two sides of the SCB film.

3. Results and discussion

SB has recently attracted wide attention in commercial food packaging as an alternative to plastics due to their low cost, biodegradability, non-toxicity and abundance of lignocellulosic availability. The current study presents the fabrication of packaging films from SB *via* delignification and phosphorylation-based functionalization route (**Figure 1**). During phosphate modification, disintegration along with the introduction of phosphate groups to the cellulose backbone occurs, resulting in a transition to a gel-like structure. The produced gels show tuneable charge content of

~500 to 1033 mmol/kg, depending upon curing time, ~ 30-90 minutes, which also resulted in variation of colour from white to pale yellow (**Figure S1**). After phosphorylation, gels were further homogenised, sonicated and cast to produce flame-retardant, transparent, mechanically robust biodegradable films with low wettability. The films were evaluated for migration under various simulated conditions and used for packaging of perishable milk-based products such as paneer, which improved the shelf life upto 14 days. The present work is a scalable approach for valorization of abundantly available SB waste into value-added packaging with improved physicochemical, functional and structural properties, making it a promising alternative to non-degradable plastic-based packaging.

3.1 Physicochemical properties and functional characteristics

3.1.1 Evaluation of charge content

Conductometric titration was performed to determine the abundance of phosphate charge in the prepared films at different curing times. **Figure S2 (a-e)** shows the conductometric curves, which were found to be divided into three regions. The first region corresponds to the highly acidic groups due to the presence of excess H+ ions, responsible for a decrease in conductivity on the addition of NaOH. The second portion corresponds to the stagnant region where neutralisation of the proton of phosphate groups takes place, and the volume of NaOH consumed in this region was used to calculate the charge content.

The third section of the conductivity curves indicates -OH group abundance, as also observed in the previously reported studies (Ablouh et al., 2021; Ait Benhamou et al., 2021). All the films exhibit a plateau region in their conductivity curves, and the length of this plateau increases as the curing time is extended. The films produced after curing for 30 (SCBF-30), 45 (SCBF-45), 60 (SCBF-60), 75 (SCBF-75) and 90 (SCBF-90) minutes of curing time exhibited the charge content of 500, 566, 700, 900 and ~1033.3 mmol/kg, respectively. The progressive increase in charge content with longer curing times suggests substitution of hydroxyl groups in the cellulose backbone with phosphate groups, which were further confirmed through FTIR and XPS spectroscopic studies, as discussed in subsequent sections.

3.1.2 FTIR spectra analysis

FTIR analysis was carried out to investigate the changes in chemical functionalization after the delignification and phosphorylation process. **Figure 2(a)** shows full range FTIR spectrographs with IR peaks at 666, 898, 1023, and 1108 cm^{-1}, which corresponds to specific molecular vibrations, namely C-C bending, C–O stretching of *β*-(1–4) glycosidic linkages, C-O-C glycosidic bonds, and stretching vibration of pyranose ring, respectively (25–28). The IR peaks observed at 1308, 1371, 2880, and 3340 cm^{-1} in **Figure 2(a) and (b)** correspond to C-H deformation, -CH_2 bending, -C-H stretching, and O-H stretching, respectively [27–30].

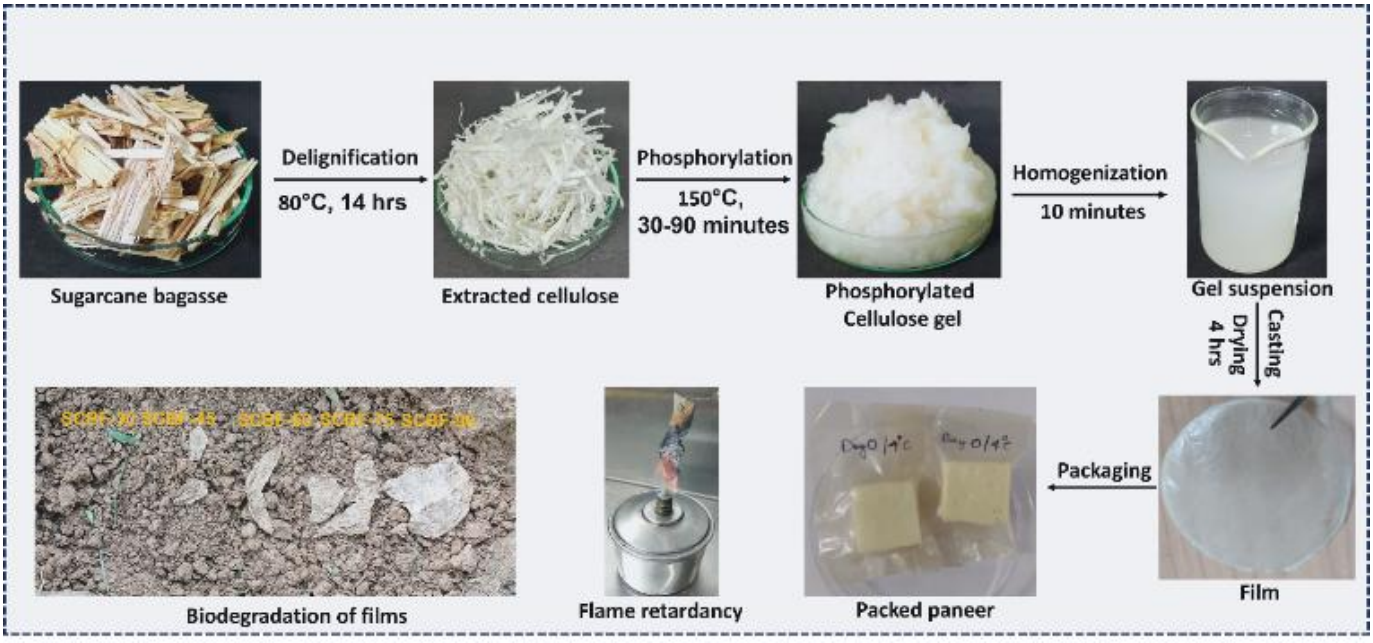

Figure 1: Illustrates a scheme for the production of phosphorylated gel from SB via delignification and phosphorylation route, which was subsequently utilised to prepare biodegradable, transparent and flame-retardant films for paneer storage.

View Article Online
DOI: 10.1039/D5FB00355E

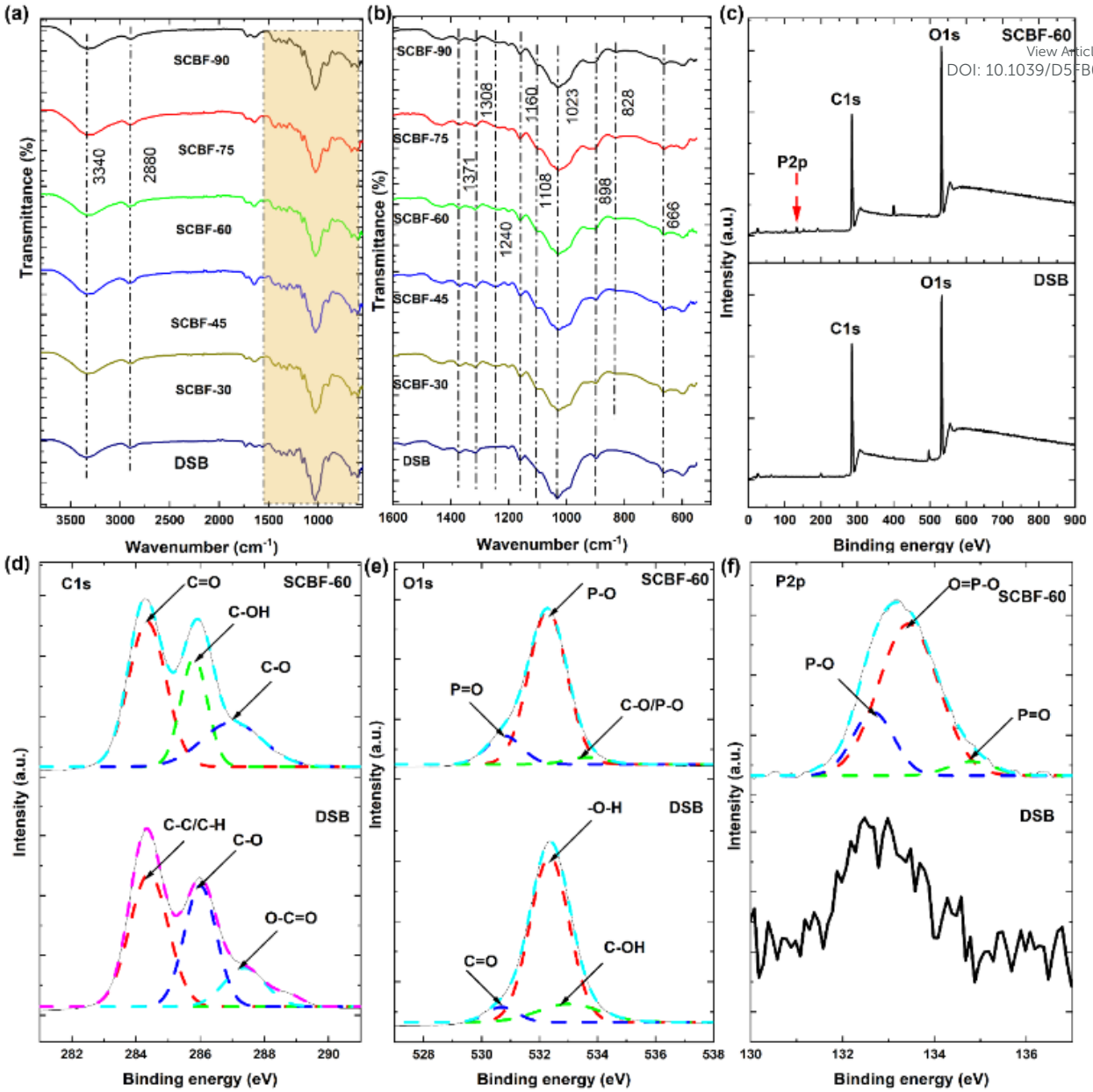

Figure 2: FTIR spectra of SCBF films in the range of (a) 600-4000 cm^{-1}, (b) 600-1600 cm^{-1}, (c) XPS survey of DSB and SCBF-60, (d) C1s, (e) O1s, and (f) P2p bond of DSB and SCBF-60.

FTIR of SCBF film shows the presence of three additional IR peaks at ~828, 1103, and 1240 cm^{-1}, which confirms the presence of P-O-C and P=O vibrational bonds, respectively, inline with the previously reported studies (Radiman and Rifathin, 2013; Suflet et al., 2006; Zhang et al., 2023; [31,32,34]). The introduction of phosphate ions into DSB resulted in the formation of P-O-C bonds, facilitating the covalent linkages of phosphate groups with the cellulose backbone, which was further confirmed through XPS studies.

3.1.3 XPS analysis

XPS analysis was performed to confirm the formation of covalent linkages and crosslinking during the phosphorylation reaction. The XPS survey of DSB exhibited two distinct peaks at 533.08 eV and 285.08 eV, which are attributed to O1s and C1s bonds, respectively (**Figure 2(c)**). In case of SCBF-60 (**Figure 2(c)**), the XPS shows three distinct peaks at 532.08 eV, 285.08 eV, and 133.08 eV, corresponding to the O1s, C1s, and P2p chemical bonds, respectively. In the present study, the C1 broad spectrum of DSB (**Figure 2(d)**) resolved into three subpeaks at the binding energies of 284.3 eV, 286 eV and 287.3 eV, representing C-H/C-C, C-O and O-C=O bonds, respectively [35,36]. The broad spectrum of C1s in SCBF-60 (**Figure 2(d)**) also resolved into three distinct sub-peaks at 284.3 eV, 285.8 eV, and 287.0 eV, corresponding to the C-C, C-OH, and C-O bonds, respectively [37,38]. The broad spectrum of O1s (DSB, **Figure 2(e)**), deconvoluted into three subpeaks at 530.6 eV, 532.3 eV and

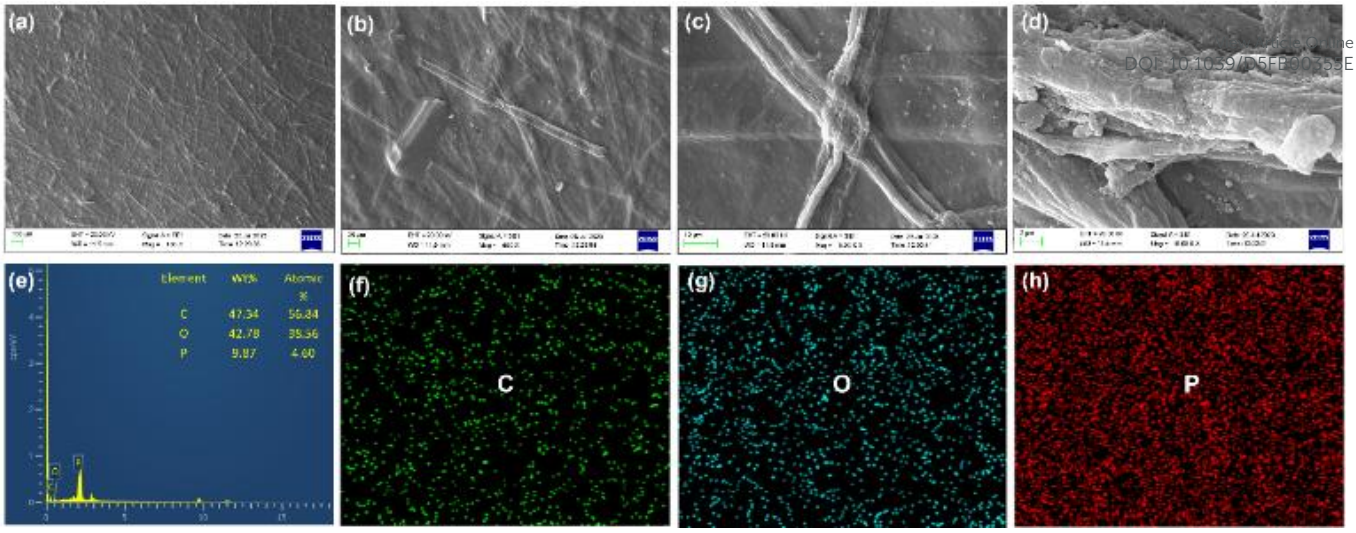

Figure 3: SEM micrograph of SCBF film (a)100X, (b) 500X, (c)3kX, (d)10kX, (e) EDS analysis with elemental mapping of (f) carbon, (g) oxygen, and (h) phosphorus, respectively.

532.8 eV, which depict C=O, -O-H, and C-OH bonds, respectively [39–41]. However, on phosphorylation, the O1s peak of SCBF-60 at 530.8 eV, 532.2 eV and 533.4 eV represents P=O, -P-O, and C-O/P-O bonds respectively (**Figure 2(e)**) [42–44]. The P2p broad spectrum of SCBF-60 (**Figure 2(f)**) is also divided into three subpeaks at 133.5 eV, 134.7 eV and 132.7 eV, corresponding to P=O, O=P-O and P-O, respectively [45–47]. However, no peaks were observed in the DSB sample for P2p (**Figure 2(f)**). The presence of phosphate bonds in O1s and P2p spectra of SCBF-60 confirms the grafting of phosphate groups in the DSB backbone. The elemental composition of SCBF-60 (**Table S1**) shows the presence of phosphate at ~ 1.7 atomic (%), which is inline with the charge determined through conductometric titration and EDX spectroscopic studies.

3.2 Morphological properties

SEM analysis was performed to investigate the surface morphology of the developed films, as shown in **Figure 3**. The SEM images of SCBF-90 (**Figures 3(a-d)**) exhibit a random distribution of cellulose fibrils with the formation of uneven and rough surfaces. The uneven distribution of fibrils with irregular structures in films can be attributed to the disintegration of the fibre's structure during homogenisation, **Figure 3(a)** and **(b)**. The solution casting of prepared gels and the heat-induced drying process resulted in a continuous and dense cellulose film layer. The presence of a network structure of cellulose fibrils with the formation of a densified system without any void spaces is expected to improve the structural properties of films, as discussed in the subsequent section. The results of EDS analysis and elemental mapping performed on SCBF-90 film are depicted in **Figure 3(e).** The elemental mapping shown in **Figures 3(f), 3(g),** and **3(h)** shows the spatial distribution of phosphorus, carbon, and oxygen elements on the film's surface, confirming the uniform phosphorylation and distribution on the DSB surface. EDS spectra show the presence of phosphate with a weight percentage of 9.37%, which is inline with the XPS and conductometric titration as discussed in the earlier section.

3.3 Structural properties

XRD was carried out to analyse the structural changes in DSB during delignification and curing-based phosphorylation and film formation process. As shown in **Figure 4(a)**, two characteristic peaks of cellulose were observed in DSB at 15.1° and 21.5°, representing the crystal planes (1-10) and (200), respectively [48,49]. After the phosphorylation reaction, a shift in peaks was observed with the peak at 15.1° of DSB shifted to 16.2° and 21.5° to 22.4°, representing (110) and (200) planes of cellulose, respectively [50,51]. The crystallinity index (C.I.) of DSB and SCBF-30 was 38.3% and 38.9%, indicating that there was no significant effect of curing time of phosphorylation on crystallinity for the first 30 minutes. Furthermore, with the increase in phosphorylation time from 45 to 75 minutes, there was no observable change in crystallinity index ~41.9%, 42.4% and 42% for SCBF-45, SCBF-60, and SCBF-75, respectively. The phosphorylation process leads to incorporation of a significant amount of phosphate groups into the amorphous region of DSB, without affecting the crystallinity significantly [27]. However, following a more extended curing period to 90 minutes, C.I. reduced to 32.3% possibly due to significant swelling and partial dissolution of DSB fibres leading to degradation, as also observed in previously reported studies [52,53].

3.4 Thermal properties

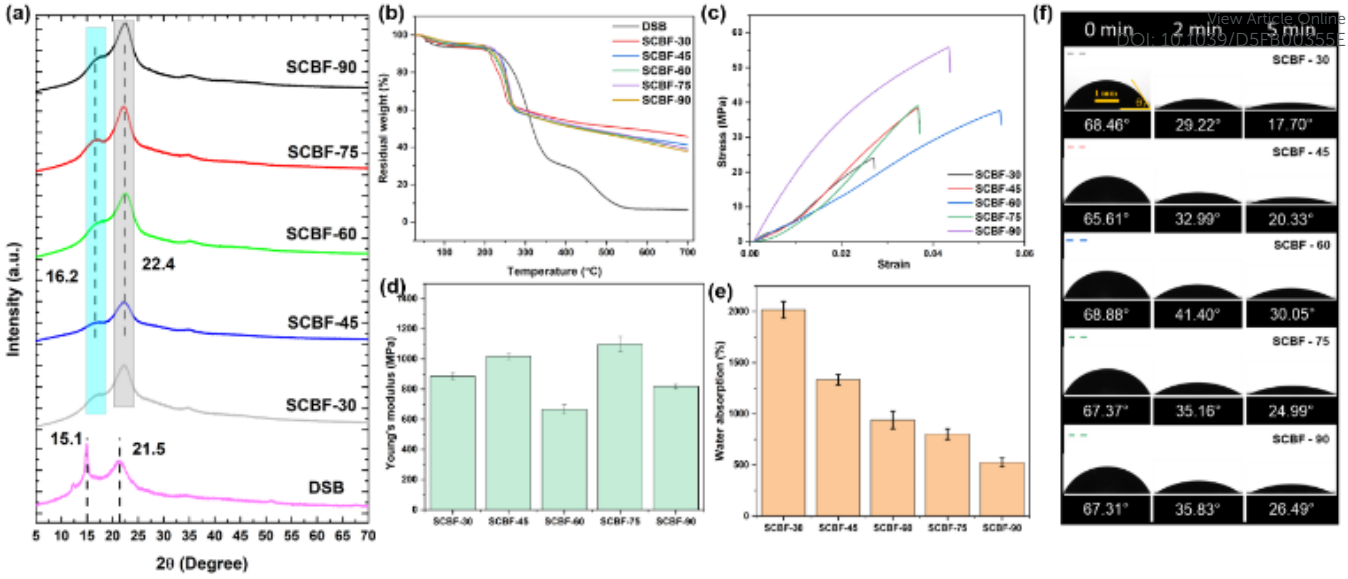

Figure 4: (a) XRD diffractogram, (b) thermogravimetric analysis, (c) tensile strength, (d) tensile modulus, (e) water absorption capacity, and (f) contact angle measurements.

To understand the effect of delignification and phosphorylation, thermogravimetric analysis was carried out for developed SCBF films at different curing times, as shown in **Figure 4(b)**. The first stage of weight loss~6.32 %, 3.56 %, 3.55 %, 4.57 %, 3.7 % and 5.1 % was observed in the 30-105°C range for DSB, SCBF-30, SCBF-45, SCBF-60, SCBF-75 and SCBF-90, respectively. The onset thermal degradation temperature (T_{onset}) was observed at 235 °C for DSB, which decreased with increasing curing time to 223 °C for SCBF-30, 231°C for SCBF-45, 215°C for SCBF-60, 230°C for SCBF-75 and 213°C for SCBF-90. DSB demonstrates two stages of decomposition; the first stage, with 51.03 % degradation occurring in the temperature range from 232-336°C and the second stage, with 19.15 % degradation observed from 430-548°C. T_{max} (50% degradation) of DSB was found to be 318°C, which on phosphorylation improved to 555°C, 427°C, 438°C, 455°C and 423°C for SCBF-30, SCBF-45, SCBF-60, SCBF-75 and SCBF-90, respectively. The residual weight percentage of SCBF-30, SCBF-45, SCBF-60, SCBF-75 and SCBF-90 at 700°C was 37.71%, 38.96%, 39.27%, 41.22% and 45.48% respectively, which significantly increased in comparison to DSB (~6.67% present at 700°C). The percentage increase in the residual weight of the developed films at 700°C was 3.31%, 4.14%, 9.31% and 20.61% for SCBF-45, SCBF-60, SCBF-75 and SCBF-90, respectively, compared to SCBF-30. The results indicate that incorporation of phosphate groups increased the yield of char residues in all films at different curing times, inline with findings reported in previous works [15,54,55].

3.5 Mechanical strength

The evaluation of the mechanical properties of SCBF films with different charge contents (**Figure 4(c & d)**) was performed to determine the strength and modulus under applied tensile load. SCBF-30, SCBF-45, SCBF-60, and SCBF-75 films show a tensile strength of 24.05, 38.37, 37.58 and 39 MPa, respectively. Interestingly, SCBF-90 films show an increase in tensile strength by almost two orders of magnitude to 55.80 MPa. These results suggest that there were 59.6%, 56.2%, 62.1% and 132% increases in the tensile strength of the samples SCBF-45, SCBF-60, SCBF-75 and SCBF-90, respectively, when compared to SCBF-30. The increased tensile strength could be attributed to enhanced crosslinking of phosphate groups during thermal-induced processing, which improves the load-bearing capacity of films. Similarly, due to higher elongation, SCBF-75 films show an improved modulus of 1098.79 MPa, followed by 1017.59 MPa for SCBF-45, 886.04 MPa for SCBF-30 and 817.58 MPa for SCBF-90 films. The cellulose films are known for their poor stability under wet conditions; however, the presence of cross-links improves the wet stability of films. In comparison to dry films, the wet strength reduced to 5, 4, 6, 9 and 10MPa for SCBF-30, SCBF-45, SCBF-60, SCBF-75 and SCBF-90 films, respectively (**Figure S8**), but is suitable enough for practical applications. The high degree of phosphate charge content and its subsequent cross-linking during processing of SCBF films [56] significantly improve strength both in dry and wet conditions, overcoming challenges associated with traditional cellulose-based packaging films.

3.6 Water absorption capacity

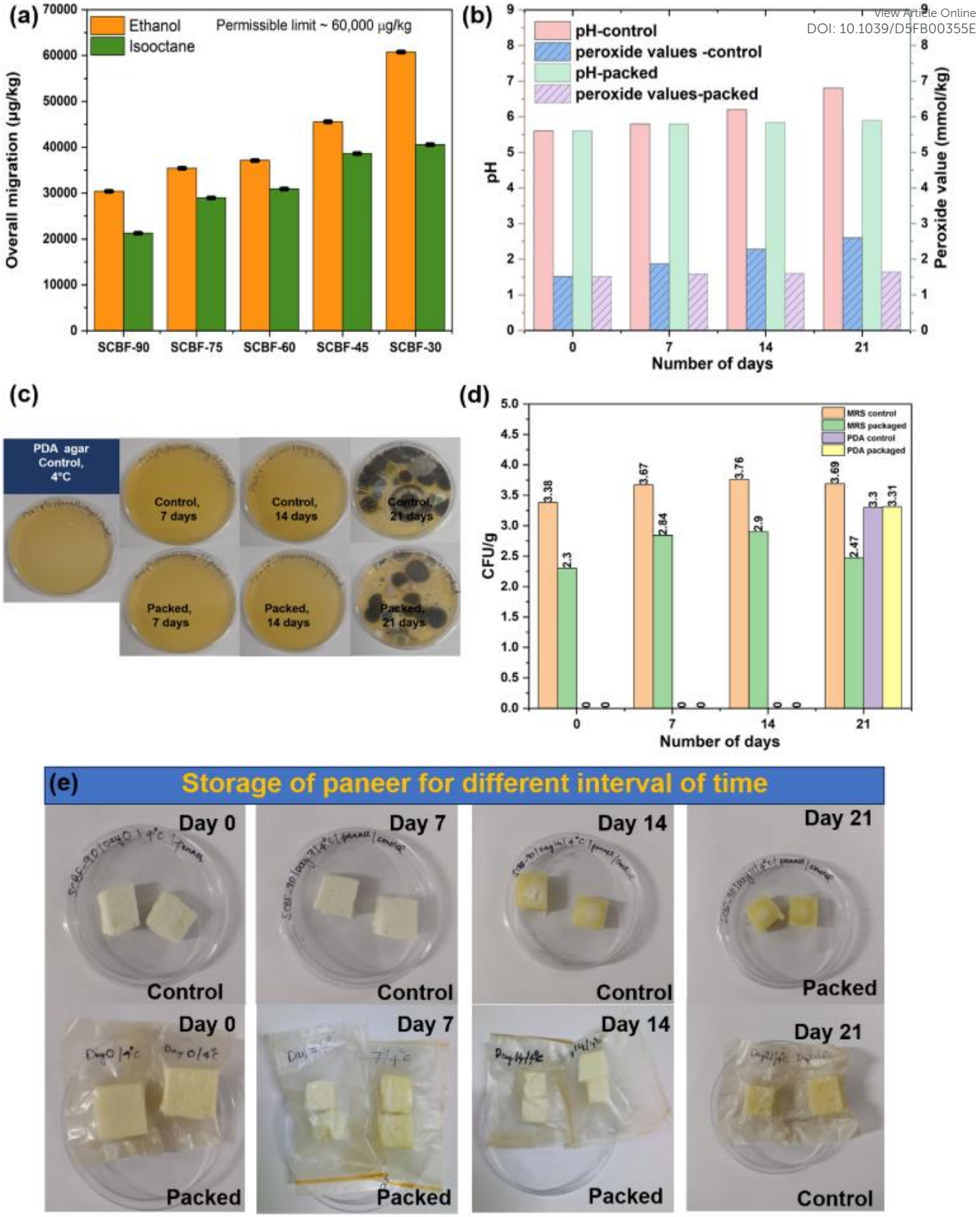

Figure 5: (a) Overall migration values measured in presence of as food simulants ethanol and isooctane, (b) changes in pH and peroxide values for control and SCBF films packed paneer, (c) PDA agar plates for growth of yeast/fungi at different time, (d) measured colonies in presence of MRS/PDA agar media, (e) changes in colour and texture of paneer when stored under control and packaged conditions at different storage time upto 21 days at 4°C.

In packaging applications, understanding the water absorption capacity and water solubility of developed cellulose films is vital to evaluate their ability to serve as barriers against moisture. In this study, the water absorption capacity of films decreased with an increase in the degree of phosphorylation and crosslinking in films. From **Figure 4(e)**, SCBF-30 shows a maximum water absorption capacity of 2016.8% which reduced to 1333%, 939.94%, 801.43%, and 525.77% for SCBF-45, SCBF-60, SCBF-75, and SCBF-90 films, respectively. Upon exposure to water, SCBF films with phosphorylated groups exhibit a propensity to interact with water; however, the presence of crosslinking restricts water infiltration, reducing their water absorption. It is also evident from the reduced water solubility of SCBF films~15-18% **(Figure S7)** when immersed in water for 24 hours. Moreover, the wet SCBF films show structural integrity and improved wettability in comparison to traditional cellulose films, as discussed in subsequent expansion.

3.7 Surface wettability of the films

The surface wettability of packaging films was studied by measuring water contact angle (CA) over a time period to evaluate their behaviour when in contact with food. As shown in **Figure 4(f)** and **S3,** SCBF-60 shows the highest initial CA of 68.88°, which almost remains unchanged with varying charge content of films to 68.46°, 65.61°, 67.37° and 67.31° for SCBF-30, SCBF-45, SCBF-75 and SCBF-90, respectively. However, the final CA after 5 minutes was found to vary depending on curing time, which reduces the wettability of films, due to the introduction of thermal-induced cross-linkages. The final CA was found to be 17.70°, 20.33°, 30.05°, 24.99° and 26.49° for SCBF-30, SCBF-45, SCBF-60, SCBF-75 and SCBF-90 films (**Figure S3**). From SEM observations, SCBF films showed a rough architecture with cellulose microfibrils on the surface, which led to easy adsorption of water droplets through capillary action. Along with its presence of hydrophilic phosphate groups led to the spreading of water droplets, with a reduction in the final CA of films with time. An increase in curing time leads to crosslinking of phosphate groups, which diminishes interaction of hydrophilic phosphate groups with water droplets, thereby reducing wettability and improving CA, making the prepared SCBF films suitable for food packaging.

3.8 Migration studies

For food packaging films, integrity in terms of leaching of components is an essential criterion for study, as it may affect the sensory properties of packed food items. Migration studies were performed with two food simulants, namely ethanol (alcoholic food simulant) and isooctane (fatty food simulant), following EU regulation No. 10/2011 (**Figure 5(a)**). For ethanol as a simulant, overall migration of SCBF-45, SCBF-60, SCBF-75, and SCBF-90 shows 45569, 37130, 35443, and 30379 µg/kg, which increased to 60759 µg/kg for SCBF-30. The migration decreased with an increase in phosphate charge groups in films, due to the formation of heat-induced cross-linkages, which improve their wet stability. On the other hand, SCBF-30 films with low charge content underwent swelling followed by disintegration due to the absence of such crosslinks during incubation for 10 days. However, the migrated components are mostly cellulosic fragments, which are known to be biocompatible and non-toxic. Similar observations with significantly lowered migration values were detected with isooctane as a non-polar solvent. The overall migration decreases with increased phosphate content as higher phosphate groups improve crosslinking ability between cellulose fibrils, resulting in lower swelling and disintegration on exposure to solvent [57]. Moreover, all the films (except SCBF-30 in ethanol) showed migration values within the EPA standard limit (60,000 micrograms/kg) and can be confirmed suitable for food packaging applications.

3.9 Flammability

The flammability test was carried out by exposing films under direct ethanol flame to determine the film's susceptibility to ignition, rate of burning and characteristics of char residue formed at the end of the test. As depicted in **Figure S4**, films such as SCBF-30, SCBF-45, and SCBF-60 catch fires quickly (2-5 seconds), and the burning rate was ~ 2.66-1.6 cm/min. However, SCBF-75 films show improved flammability with slow burning upto 15 seconds, and reduced burning rate of 0.571 cm/sec, by almost two orders of magnitude. The burning rate further reduced the maximum for SCBF-90 (0.15 cm/sec), possibly due to the highest phosphate charge (1033.33 mmol/kg). During the burning of films, the surface becomes black with the formation of char; however, it retains its dimensional and structural integrity. The char residue left after flammability experiments was 21.28, 19.7, 33.9, 36.9 and 39.7% for SCBF-30, SCBF-45, SCBF-60, SCBF-75 and SCBF-90, respectively, which is inline with TGA studies, discussed in the previous section.

3.10 Packaging of the paneer, evaluation of its shelf life and water vapour permeability

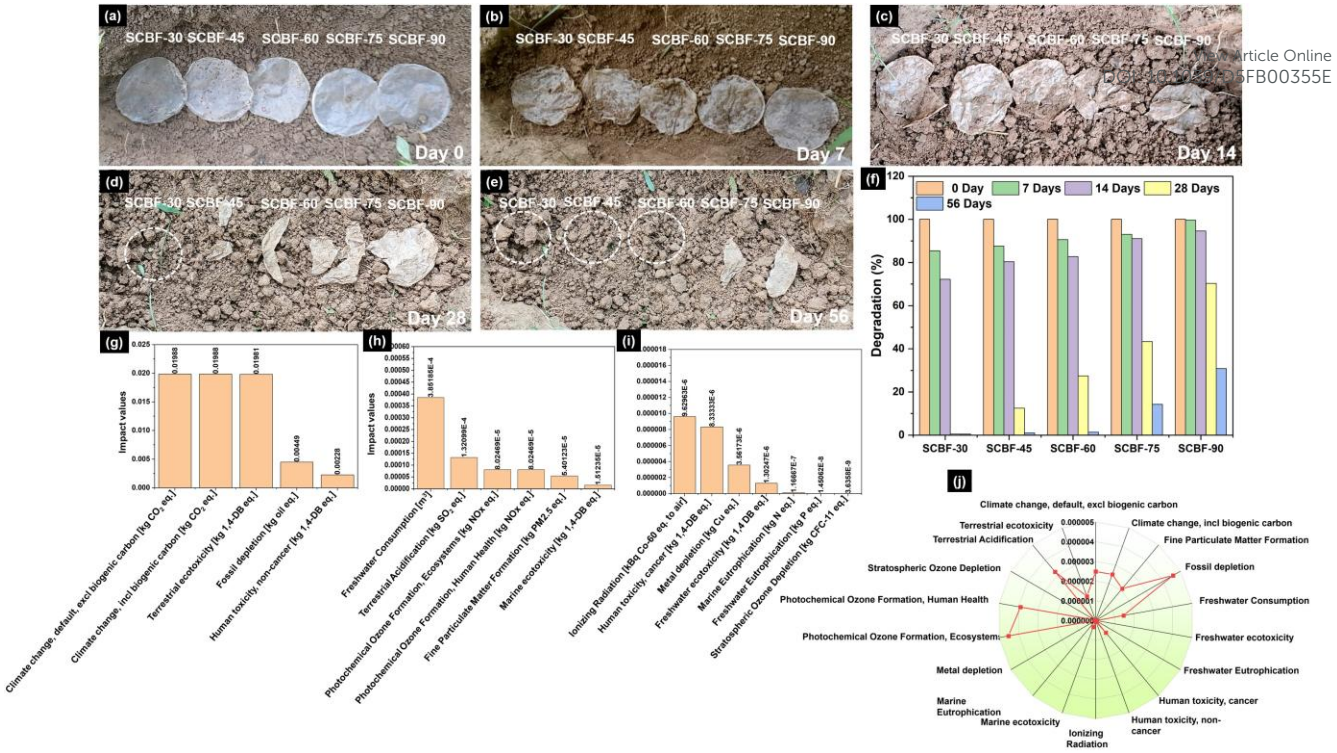

Figure 6: Photographs of the films (a-e) examine physical changes occurring during different intervals of soil burial to study the process of biodegradation, (f) biodegradation percentage at different intervals of soil burial, (h-i) mid-point results generated from the production of a single SCBF film and (g) normalisation of the mid-point results.

The biodegradable food packets of SCBF-90 films with dimensions ~5 cm × 1.5 cm were fabricated, which were utilised for packaging paneer at 4°C for 21 days (shown in **Figure 5(g))**. Under packed conditions, the colour of paneer changed from natural white to a lighter shade of yellow in both control and packaging conditions, depending upon storage time. Furthermore, an alteration in the consistency of paneer was noted as it transitioned from soft and spongy to a more rigid form in the case of the control sample within 7 days of storage time. In contrast, paneer under packed condition remained soft and spongy even after 21 days of storage. During the 21-day storage period, a change in pH was observed from 5.6 to 6.8 in the control, whereas a negligible change was observed in packaged samples. Furthermore, there was an increase in peroxide value of paneer from 1.52 to 2.60 mmol/kg in the control after 14 days; however, packaged samples show a slight increase in peroxide value from 1.52 to 1.64 mmol/kg even after 21 days of storage time. Microbiological evaluations were performed on samples collected at different time intervals (0, 7, 14, and 21 days) to evaluate the growth of potentially harmful pathogenic bacteria that could affect human health. The investigation involved the assessment of the growth of lactic acid and coliform bacteria by using selective MRS and VRBA agar plates, respectively. According to data in **Figure 5(d)**, the control sample exhibited 3.38, 3.67, 3.76, and 3.69 log CFU/g of lactic acid bacteria after being stored for 0,7,14 and 21 days, respectively. On the other hand, packaged samples showed reduced growth of lactic acid bacteria with 2.30, 2.84, 2.90, and 2.47 log CFU/g under identical storage durations.

Significantly, the selective VRBA, XLD agar and PALCAM agar plates exhibited no detectable growth of pathogenic coliform bacteria, *Salmonella* and *Listeria* species during the entire 21-day storage period (**Figures S6)**. Additionally, the absence of *Pseudomonas* species was confirmed as there was no observable growth on the *Pseudomonas* agar plates, as depicted in **Figure S6**. There was no visible growth of yeast or fungi in samples stored for 14 days in PDA agar. However, it was observed that both control and packaged samples exhibited growth of 3.30 and 3.11 log CFU/g of yeast/fungus, respectively, after 21 days of storage **Figure 5(d)**. This implies that the developed SCBF-90 films, when used for the packaging of paneer, could maintain their suitability for consumption upto 14 days.

Barrier properties are essential for food preservation. It is vital to limit water vapour transfer through the packaging film to prevent the growth of microorganisms, food oxidation, and ultimately spoilage. The films show minimal porosity, as evidenced by the SEM image; therefore, water vapour transport mainly occurs through the dense polymer matrix rather than pores or voids. In these systems, permeation follows the solution-diffusion model, where water vapour molecules adsorb onto the film surface, dissolve within the matrix, diffuse through it, and desorb on the opposite side. The data presented in **Table S3** display the WVTR and WVP values for SCBF films (30-90), with SCBF-30 showing the lowest and SCBF-90 the highest. The WVTR decreases progressively from 58.63 g/m².24h for SCBF-30 to 34.22 g/m².24h for SCBF-90. Similarly, WVP

declines from 9.42 × 10^{-12} gm/m²·s·Pa for SCBF-30 to 5.50 × 10^{-12} gm/m²·s·Pa for SCBF-90. The WVTR reduces by around 41% from SCBF-30 (58.63 g/m².24h) to SCBF-90 (34.22 g/m².24h), indicating a notable enhancement in barrier performance with increased phosphate content. The trends seen in WVTR and WVP are due to the effect of phosphate content on the molecular structure of the film, particularly its crosslinking ability. Higher phosphate levels improve the crosslinking of the polymer matrix, resulting in a denser, more compact network through covalent or ionic bonds between polymer chains, thereby reducing the free volume available for water vapour molecules to diffuse.

In real-world applications, such as food packaging created from phosphorylated agricultural waste, the increased WVP of these films can be problematic because effective moisture barriers are essential for preventing food spoiling and microbiological development. To tackle this issue, exploring the addition of various components, including hydrophobic polymers, nanomaterials, or lipid-based coatings, may prove beneficial in improving the water vapour barrier properties while still preserving the sustainability advantages associated with agricultural waste-derived cellulose. Current investigations are examining these modifications, and the results will be detailed in upcoming publications to offer a thorough assessment of enhanced film compositions for practical uses.

3.11 Biodegradation of SCBF films

SCBF films were introduced into garden soil to examine the effects of phosphorylation on biodegradability, change in physical appearance and subsequent weight loss was monitored upto 56 days (shown in **Figure 6(a-e)**). As depicted in **Figure 6(f),** SCBF-30, SCBF-45, SCBF-60, SCBF-75, and SCBF-90 demonstrated the most substantial degradation of 14.5%, 12.40%, 9.41%, 6.95%, and 0.35% at 7 days, respectively, with no notable film disintegration. However, SCBF-30 and SCBF-45 films underwent disintegration within 14 days, leading to enhanced biodegradation of 27.83% and 19.66%, respectively. On other hand, SCBF-60, SCBF-75, and SCBF-90 showed lowered degradation of 17.28%, 8.92% and 5.39%, respectively with minor disintegration (**Figure 6(c)**). However, after 28 days of burial, all films underwent significantly increased biodegradation, leading to observable disintegration **(Figure 6(d))**. After 28 days, the biodegradation of SCBF-30 and SCBF-45 was 99.55% and 87.56% respectively. On the other hand, SCBF-60, SCBF-75, and SCBF-90 films demonstrated lowered biodegradation of 72.60%, 56.67%, and 29.72%, respectively, following a 28-day burial period. The SCBF-60 completely degraded on 56 days of burial; however, SCBF-75 and SCBF-90 showed 85.76% and 69.22% biodegradation **(Figure 6(e))**. The lowered degradation rate of SCBF-90 is possibly due to the presence of a higher degree of thermally induced phosphate-based cross-linkages. These findings suggest that phosphorylation does not modify the intrinsic biodegradable properties of cellulose; however, the rate is controlled by the degree of cross-linking. When SCBF films are buried in the soil, the presence of moisture leads to their swelling, and microbial activity results in biodegradation of films [57–59]. The SCBF-30 demonstrated the highest and most rapid degradation due to lower phosphate content, increased water absorption capacity, and reduced crosslinking.

3.12 LCA of SCBF-film

Figures 6(g), 6(h), and **6(i)** depict the environmental impacts resulting from the delignification, phosphorylation and production process of SCBF film. As illustrated in **Figure 6(g),** the impact category of climate change (including and excluding biogenic carbon) exhibited the highest impacts, reaching 0.0198 kg CO_2 eq., surpassing all other categories. The primary factor contributing to the significant influence on climate change categories is likely attributed to the substantial release of greenhouse gases during electricity generation from hard coal. The impacts generated in the terrestrial ecotoxicity category was almost similar to the climate change category ~0.0198 kg DB eq. The primary factor influencing these increased effects is the utilisation of chemical reagents during pre-treatment, functionalization and processing of SB. Freshwater eutrophication and stratospheric ozone depletion exhibited the lowest impact values, measuring 1.45 × 10^{-8} kg P eq. and 3.63 × 10^{-8} kg CFC-11 eq., respectively. The LCA study suggests that environmental impacts resulting from the treatment of SB waste are relatively less harmful and similar to the impact generated in the traditional manufacturing of spray-deposited cellulose nanofiber films [60].

3.13 Normalisation of mid-point results

The midpoint results obtained during the production of SCBF films were standardised to identify the dominant environmental impact categories. **Figure 6(j)** demonstrates that among 18 categories, fossil depletion, photochemical ozone formation, and terrestrial acidification substantially contribute to the environmental impact. Fossil depletion exhibits the highest impact value, measuring 4.56 × 10^{-6} kg oil eq., while photochemical ozone formation and terrestrial acidification have impact values of 4.52 × 10^{-6} kg NOx eq. and 3.22 × 10^{-6} kg SO_2 eq., respectively. The normalised midpoint results highlight fossil depletion, photochemical ozone formation, and terrestrial acidification as the dominant categories, and were subsequently chosen for sensitivity analysis.

3.14 Sensitivity analysis

A sensitivity analysis is conducted on predominant ecological categories associated with the production of SCBF film to assess the variation in impact values on varying inputs of key factors. **Table S2** depicts the effects of a 10% increase and decrease of 8% in the input values of key parameters, namely electricity, delignification, and phosphorylation, on dominant environmental categories. An increase in electricity by 10% leads to proportional impacts in photochemical ozone formation (9.63%), terrestrial acidification

(9.81%), and 10% fossil depletion. The primary cause of this phenomenon can be attributed to the significant energy consumption associated with processes derived from the combustion of hard coal. A reduction of 8% in electricity input resulted in corresponding decreases by -7.84%, -7.69%, and -7.48% of fossil depletion, photochemical ozone formation, and terrestrial acidification, respectively. In addition, when the input of delignification was increased by 10%, impact values of fossil depletion, photochemical ozone formation, and terrestrial acidification increased by 5.09%, 5.38%, and 5.61%, respectively. Nevertheless, a reduction of 8% in input led to a decrease of -4.13%, -3.85%, and -4.21% in the impact of fossil depletion, photochemical ozone formation, and terrestrial acidification categories, respectively. Additionally, when the input of the phosphorylation process was increased by 10%, there was a corresponding increase of 1.79%, 2.31%, and 1.87% in the impact values in the categories of fossil depletion, photochemical ozone formation, and terrestrial acidification, respectively. The sensitivity analysis conducted for the production of SCBF film reveals that electricity consumption emerges as the most crucial factor of significance. This phenomenon is apparent as the primary environmental categories display consistent fluctuations in response to proportional increments or decrements in electricity consumption during production.

4. Conclusion

The current study presents novel, eco-friendly, and sustainable routes for valorising SB waste into value-added phosphorylated gels and films for food packaging applications. The study utilises low-cost agro-based chemicals through a scalable approach for phosphorylating SB biomass into cellulose gel following delignification and phosphorylation routes. The developed process yields a gel of ~85%, with tuneable charge content 500-1130 mmol/kg, depending upon curing time of 30-90 min and undergoes a transition in colour from transparent to light yellow. The physicochemical and structural properties were found to depend on the degree of phosphorylation and heat-induced cross-linkages during curing, which were confirmed through FTIR and XPS studies. The gels transformed into films through the solution casting method exhibit exceptional mechanical properties, water stability, thermal stability, and flame retardancy. Interestingly, the SCBF films show improved wet strength and surface wettability compared to traditional cellulose films due to the presence of phosphate-based cross-linkages, which makes them suitable for packaging applications. The films were subsequently used for packaging perishable food items such as paneer, improving its shelf life by 14 days, minimising the risk of microbial contamination and maintaining minimal alterations in pH and peroxide values. Interestingly, the migration values of SCBF films were within the standard limits and showed improved biodegradability within ~56 days. Moreover, LCA studies conducted on the production of SCBF films demonstrate reduced carbon dioxide (CO_2) emissions, indicating that the developed process is environmentally sustainable with a lower carbon footprint. The present study opens up new avenues for up-conversion of waste biomass following a scalable delignification-*cum*-phosphorylation approach for the production of biodegradable films for potential food packaging applications.

Author contributions

R.R. led the original draft's writing, carried out the experiments, curated the data, performed formal analysis, and contributed to the technique design. P.D. formulated the initial concept, oversaw the project, and handled the overall administration of the project. C.K. conducted and analyzed the contact angle measurements.

Conflicts of interest

There are no conflicts to declare.

Data availability

The information supporting this article has been incorporated into the manuscript. Additional details may be obtained from the corresponding author (P.D.).

Acknowledgements

R.R. is thankful for the fellowship from the Ministry of Education (MOE), Govt of India (GoI). Dhar with Ramalingaswami fellowship and Har Govind Khorana-Innovative Young Biotechnologist Fellowship (IYBF), thanks DBT for providing research project funding (DBTHRDPMU/JRF/BET-20/I/2020/AL/07 and BT/HRD/35/02/2006) for carrying out the research work. P.D. grateful to Department of Science and Technology (DST), Government of India (DST/INT/JSPS/P-381/2024(G)) and National Technical Textiles Mission (NTTM), Ministry of Textiles, Government of India (EDU-24-00087) for the research financial support provided.

References

(1) Tardy, B. L.; Richardson, J. J.; Greca, L. G.; Guo, J.; Bras, J.; Rojas, O. J. Advancing Bio-Based Materials for Sustainable Solutions to Food Packaging. *Nat Sustain* **2023**, *6* (4), 360–367. https://doi.org/10.1038/s41893-022-01012-5.

(2) Freixo, R.; Casanova, F.; Ribeiro, A. B.; Pereira, C. F.; Costa, E. M.; Pintado, M. E.; Ramos, Ó. L. Extraction Methods and Characterization of Cellulose Fractions from a Sugarcane By-Product for Potential Industry Applications. *Industrial Crops and Products* **2023**, *197*, 116615. https://doi.org/10.1016/j.indcrop.2023.116615.

(3) Thai, Q. B.; Nguyen, S. T.; Ho, D. K.; Tran, T. D.; Huynh, D. M.; Do, N. H. N.; Luu, T. P.; Le, P. K.; Le, D. K.; Phan-Thien, N.;

Duong, H. M. Cellulose-Based Aerogels from Sugarcane Bagasse for Oil Spill-Cleaning and Heat Insulation Applications. *Carbohydrate Polymers* **2020**, *228*, 115365. https://doi.org/10.1016/j.carbpol.2019.115365.

(4) Carvalho, J. T. T.; Milani, P. A.; Consonni, J. L.; Labuto, G.; Carrilho, E. N. V. M. Nanomodified Sugarcane Bagasse Biosorbent: Synthesis, Characterization, and Application for Cu(II) Removal from Aqueous Medium. *Environ Sci Pollut Res* **2021**, *28* (19), 24744–24755. https://doi.org/10.1007/s11356-020-11345-3.

(5) Mehrzad, S.; Taban, E.; Soltani, P.; Samaei, S. E.; Khavanin, A. Sugarcane Bagasse Waste Fibers as Novel Thermal Insulation and Sound-Absorbing Materials for Application in Sustainable Buildings. *Building and Environment* **2022**, *211*, 108753. https://doi.org/10.1016/j.buildenv.2022.108753.

(6) Yang, Y.; Liu, H.; Wu, M.; Ma, J.; Lu, P. Bio-Based Antimicrobial Packaging from Sugarcane Bagasse Nanocellulose/Nisin Hybrid Films. *International Journal of Biological Macromolecules* **2020**, *161*, 627–635. https://doi.org/10.1016/j.ijbiomac.2020.06.081.

(7) Sharma, M.; Das, P. P.; Sood, T.; Chakraborty, A.; Purkait, M. K. Ameliorated Polyvinylidene Fluoride Based Proton Exchange Membrane Impregnated with Graphene Oxide, and Cellulose Acetate Obtained from Sugarcane Bagasse for Application in Microbial Fuel Cell. *Journal of Environmental Chemical Engineering* **2021**, *9* (6), 106681. https://doi.org/10.1016/j.jece.2021.106681.

(8) de Almeida, M. A.; Colombo, R. Production Chain of First-Generation Sugarcane Bioethanol: Characterization and Value-Added Application of Wastes. *Bioenerg. Res.* **2023**, *16* (2), 924–939. https://doi.org/10.1007/s12155-021-10301-4.

(9) Kumar, H.; Gehlaut, A. K.; Gaur, A.; Park, J.-W.; Maken, S. Development of Zinc-Loaded Nanoparticle Hydrogel Made from Sugarcane Bagasse for Special Medical Application. *J Mater Cycles Waste Manag* **2020**, *22* (6), 1723–1733. https://doi.org/10.1007/s10163-020-01054-x.

(10) Chen, W.; Wang, H.; Lan, W.; Li, D.; Zhang, A.; Liu, C. Construction of Sugarcane Bagasse-Derived Porous and Flexible Carbon Nanofibers by Electrospinning for Supercapacitors. *Industrial Crops and Products* **2021**, *170*, 113700. https://doi.org/10.1016/j.indcrop.2021.113700.

(11) Tang, S.; Chen, Z.; Chen, F.; Lai, X.; Wei, Q.; Chen, X.; Jiang, C. Extraction and Surface Functionalization of Cellulose Nanocrystals from Sugarcane Bagasse. *Molecules* **2023**, *28* (14), 5444. https://doi.org/10.3390/molecules28145444.

(12) Huong, L. M.; Trung, T. Q.; Tuan, T. T.; Viet, N. Q.; Dat, N. M.; Nghiem, D. G.; Thinh, D. B.; Tinh, N. T.; Oanh, D. T. Y.; Phuong, N. T.; Nam, H. M.; Phong, M. T.; Hieu, N. H. Surface Functionalization of Graphene Oxide by Sulfonation Method to Catalyze the Synthesis of Furfural from Sugarcane Bagasse. *Biomass Conv. Bioref.* **2022**. https://doi.org/10.1007/s13399-021-02272-5.

(13) Bansal, M.; Kumar, D.; Chauhan, G. S.; Kaushik, A.; Kaur, G. Functionalization of Nanocellulose to Quaternized Nanocellulose Tri-Iodide and Its Evaluation as an Antimicrobial Agent. *International Journal of Biological Macromolecules* **2021**, *190*, 1007–1014. https://doi.org/10.1016/j.ijbiomac.2021.08.228.

(14) Lu, P.; Yang, Y.; Liu, R.; Liu, X.; Ma, J.; Wu, M.; Wang, S. Preparation of Sugarcane Bagasse Nanocellulose Hydrogel as a Colourimetric Freshness Indicator for Intelligent Food Packaging. *Carbohydrate Polymers* **2020**, *249*, 116831. https://doi.org/10.1016/j.carbpol.2020.116831.

(15) Messa, L. L.; Faez, R.; Hsieh, Y.-L. Phosphorylated Cellulose Nanofibrils from Sugarcane Bagasse with pH Tunable Gelation. *Carbohydrate Polymer Technologies and Applications* **2021**, *2*, 100085. https://doi.org/10.1016/j.carpta.2021.100085.

(16) Ji, Q.; Yu, X.; Chen, L.; Yarley, O. P. N.; Zhou, C. Facile Preparation of Sugarcane Bagasse-Derived Carbon Supported MoS2 Nanosheets for Hydrogen Evolution Reaction. *Industrial Crops and Products* **2021**, *172*, 114064. https://doi.org/10.1016/j.indcrop.2021.114064.

(17) Gopalakrishnan, R.; Kaveri, R. Using Graphene Oxide to Improve the Mechanical and Electrical Properties of Fiber-Reinforced High-Volume Sugarcane Bagasse Ash Cement Mortar. *Eur. Phys. J. Plus* **2021**, *136* (2), 202. https://doi.org/10.1140/epjp/s13360-021-01179-4.

(18) Lin, T. H.; Thang, T. Q.; An, H.; Hai, N. D.; Duy, P. H. A.; Duyen, D. T. M.; Oanh, D. T. Y.; Van Tuyen, N.; Nam, H. M.; Phong, M. T. Synthesis of TiO2-Doped Carbon Aerogel from Sugarcane Bagasse for High Efficiency of Photodegradation of Methylene Blue in the Water. *Vietnam Journal of Chemistry* **2023**, *61* (2), 227–237.

(19) Patoary, M. K.; Islam, S. R.; Farooq, A.; Rashid, M. A.; Sarker, S.; Hossain, Md. Y.; Rakib, M. A. N.; Al-Amin, Md.; Liu, L. Phosphorylation of Nanocellulose: State of the Art and Prospects. *Industrial Crops and Products* **2023**, *201*, 116965. https://doi.org/10.1016/j.indcrop.2023.116965.

(20) Messa, L. L.; Hsieh, Y.-L.; Faez, R. Sugarcane Bagasse Derived Phosphorylated Cellulose as Substrates for Potassium Release Induced by Phosphates Surface and Drying Methods. *Industrial Crops and Products* **2022**, *187*, 115350. https://doi.org/10.1016/j.indcrop.2022.115350.

(21) Gan, I.; Chow, W. S. Tailoring Chemical, Physical, and Morphological Properties of Sugarcane Bagasse Cellulose Nanocrystals via Phosphorylation Method. *Journal of Natural Fibers* **2021**, *18* (10), 1448–1459. https://doi.org/10.1080/15440478.2019.1691120.

(22) Meng, L.; Xi, J.; Bian, H.; Xiao, H.; Wu, W. Nanocellulose/Natural Rubber Latex Composite Film with High Barrier and Preservation Properties. *Sustainable Chemistry and Pharmacy* **2024**, *37*, 101399. https://doi.org/10.1016/j.scp.2023.101399.

(23) Abdelghaffar, F. Biosorption of Anionic Dye Using Nanocomposite Derived from Chitosan and Silver Nanoparticles Synthesized via Cellulosic Banana Peel Bio-Waste. *Environmental Technology & Innovation* **2021**, *24*, 101852. https://doi.org/10.1016/j.eti.2021.101852.

(24) Md Salim, R.; Asik, J.; Sarjadi, M. S. Chemical Functional Groups of Extractives, Cellulose and Lignin Extracted from Native Leucaena Leucocephala Bark. *Wood Sci Technol* **2021**, *55* (2), 295–313. https://doi.org/10.1007/s00226-020-01258-2.

(25) Caputo, D.; Fusco, C.; Nacci, A.; Palazzo, G.; Murgia, S.; D'Accolti, L.; Gentile, L. A Selective Cellulose/Hemicellulose Green Solvents Extraction from Buckwheat Chaff. *Carbohydrate Polymer Technologies and Applications* **2021**, *2*, 100094. https://doi.org/10.1016/j.carpta.2021.100094.

(26) Akhlaq, M.; Maqsood, H.; Uroos, M.; Iqbal, A. A Comparative Study of Different Methods for Cellulose Extraction from Lignocellulosic Wastes and Conversion into Carboxymethyl

Cellulose. *ChemistrySelect* **2022**, *7* (29), e202201533. https://doi.org/10.1002/slct.202201533.

(27) Ait Benhamou, A.; Kassab, Z.; Nadifiyine, M.; Salim, M. H.; Sehaqui, H.; Moubarik, A.; El Achaby, M. Extraction, Characterization and Chemical Functionalization of Phosphorylated Cellulose Derivatives from Giant Reed Plant. *Cellulose* **2021**, *28* (8), 4625–4642.

(28) Huang, S.; Li, S.; Lu, X.; Wang, Y. Modification of Cellulose Nanocrystals as Antibacterial Nanofillers to Fabricate Rechargeable Nanocomposite Films for Active Packaging. *ACS Sustainable Chem. Eng.* **2022**, *10* (28), 9265–9274. https://doi.org/10.1021/acssuschemeng.2c01793.

(29) Liang, W.; Jiang, M.; Zhang, J.; Dou, X.; Zhou, Y.; Jiang, Y.; Zhao, L.; Lang, M. Novel Antibacterial Cellulose Diacetate-Based Composite 3D Scaffold as Potential Wound Dressing. *Journal of Materials Science & Technology* **2021**, *89*, 225–232. https://doi.org/10.1016/j.jmst.2020.12.007.

(30) Hernández-Becerra, E.; Osorio, M.; Marín, D.; Gañán, P.; Pereira, M.; Builes, D.; Castro, C. Isolation of Cellulose Microfibers and Nanofibers by Mechanical Fibrillation in a Water-Free Solvent. *Cellulose* **2023**, *30* (8), 4905–4923. https://doi.org/10.1007/s10570-023-05162-3.

(31) Radiman, C. L.; Rifathin, A. Preparation of Phosphorylated Nata-de-Coco for Polymer Electrolyte Membrane Applications. *Journal of Applied Polymer Science* **2013**, *130* (1), 399–405. https://doi.org/10.1002/app.39180.

(32) Zhang, N.; Li, J.; Tian, B.; Zhang, J.; Li, T.; Li, Z.; Wang, Y.; Liu, Z.; Zhao, H.; Ma, F. Phosphorylated Cellulose Carbamate for Highly Effective Capture of U(VI). *J Radioanal Nucl Chem* **2023**, *332* (1), 173–183. https://doi.org/10.1007/s10967-022-08678-3.

(33) Suflet, D. M.; Chitanu, G. C.; Popa, V. I. Phosphorylation of Polysaccharides: New Results on Synthesis and Characterisation of Phosphorylated Cellulose. *Reactive and Functional Polymers* **2006**, *66* (11), 1240–1249. https://doi.org/10.1016/j.reactfunctpolym.2006.03.006.

(34) Jiang, G.; Qiao, J.; Hong, F. Application of Phosphoric Acid and Phytic Acid-Doped Bacterial Cellulose as Novel Proton-Conducting Membranes to PEMFC. *International Journal of Hydrogen Energy* **2012**, *37* (11), 9182–9192. https://doi.org/10.1016/j.ijhydene.2012.02.195.

(35) Wang, W.; Niu, B.; Liu, R.; Chen, H.; Fang, X.; Wu, W.; Wang, G.; Gao, H.; Mu, H. Development of Bio-Based PLA/Cellulose Antibacterial Packaging and Its Application for the Storage of Shiitake Mushroom. *Food Chemistry* **2023**, *429*, 136905. https://doi.org/10.1016/j.foodchem.2023.136905.

(36) Ma, H.; Liu, Z.; Lou, J.; Ding, Q.; Jiang, Y.; Li, X.; Han, W. Bacterial Cellulose/MWCNT Coatings for Highly Sensitive and Flexible Paper-Based Humidity Sensors. *Cellulose* **2023**, *30* (2), 1193–1204. https://doi.org/10.1007/s10570-022-04960-5.

(37) Dhanya, V.; Arunraj, B.; Rajesh, N. Prospective Application of Phosphorylated Carbon Nanofibers with a High Adsorption Capacity for the Sequestration of Uranium from Ground Water. *RSC Advances* **2022**, *12* (21), 13511–13522. https://doi.org/10.1039/D2RA02031A.

(38) Zanata, L.; Tofanello, A.; Martinho, H. S.; Souza, J. A.; Rosa, D. S. Iron Oxide Nanoparticles–Cellulose: A Comprehensive Insight on Nanoclusters Formation. *J Mater Sci* **2022**, *57* (1), 324–335. https://doi.org/10.1007/s10853-021-06564-z.

(39) Grzyb, B.; Hildenbrand, C.; Berthon-Fabry, S.; Bégin, D.; Job, N.; Rigacci, A.; Achard, P. Functionalisation and Chemical Characterisation of Cellulose-Derived Carbon Aerogels. *Carbon* **2010**, *48* (8), 2297–2307. https://doi.org/10.1016/j.carbon.2010.03.005.

(40) Yang, W.; Tian, H.; Liao, J.; Wang, Y.; Liu, L.; Zhang, L.; Lu, A. Flexible and Strong Fe3O4/Cellulose Composite Film as Magnetic and UV Sensor. *Applied Surface Science* **2020**, *507*, 145092. https://doi.org/10.1016/j.apsusc.2019.145092.

(41) Liu, C.; Gao, C.; Wang, W.; Wang, X.; Wang, Y.; Hu, W.; Rong, Y.; Hu, Y.; Guo, L.; Mei, A.; Han, H. Cellulose-Based Oxygen-Rich Activated Carbon for Printable Mesoscopic Perovskite Solar Cells. *Solar RRL* **2021**, *5* (9), 2100333. https://doi.org/10.1002/solr.202100333.

(42) Ma, Z.; Zhang, Z.; Zhao, F.; Wang, Y. A Multifunctional Coating for Cotton Fabrics Integrating Superior Performance of Flame-Retardant and Self-Cleaning. *Adv Compos Hybrid Mater* **2022**, *5* (4), 2817–2833. https://doi.org/10.1007/s42114-022-00464-9.

(43) Wang, W.; Kan, Y.; Pan, H.; Pan, Y.; Li, B.; Liew, K. M.; Hu, Y. Phosphorylated Cellulose Applied for the Exfoliation of LDH: An Advanced Reinforcement for Polyvinyl Alcohol. *Composites Part A: Applied Science and Manufacturing* **2017**, *94*, 170–177. https://doi.org/10.1016/j.compositesa.2016.11.031.

(44) Lokhande, K. D.; Bhakare, M. A.; Bondarde, M. P.; Dhumal, P. S.; Some, S. Bio-Derived Efficient Flame-Retardants for Cotton Fabric. *Cellulose* **2022**, *29* (6), 3583–3593. https://doi.org/10.1007/s10570-022-04478-w.

(45) Yang, S.; Wang, Z.; Liu, Z.; Ji, N.; Wu, Y. In Situ Synthesis and Self-Assembly of Acid Nanospheres with Anti-Leach Properties for the Development of Fire-Resistant Wood. *Journal of Industrial and Engineering Chemistry* **2023**, *119*, 414–427. https://doi.org/10.1016/j.jiec.2022.11.064.

(46) Shi, X.-H.; Xie, W.-M.; Wu, S.-J.; Liu, Q.-Y.; De La Vega, J.; Wang, D.-Y. Facile Fabrication of High-Efficiency Reactive Flame Retardant toward Cotton Fabric with Good Hand Feeling and High Fire Safety. *Cellulose* **2023**, *30* (11), 7313–7328. https://doi.org/10.1007/s10570-023-05306-5.

(47) Xu, J.; Niu, Y.; Xie, Z.; Liang, F.; Guo, F.; Wu, J. Synergistic Flame Retardant Effect of Carbon Nanohorns and Ammonium Polyphosphate as a Novel Flame Retardant System for Cotton Fabrics. *Chemical Engineering Journal* **2023**, *451*, 138566. https://doi.org/10.1016/j.cej.2022.138566.

(48) Haouache, S.; Jimenez-Saelices, C.; Cousin, F.; Falourd, X.; Pontoire, B.; Cahier, K.; Jérome, F.; Capron, I. Cellulose Nanocrystals from Native and Mercerized Cotton. *Cellulose* **2022**, *29* (3), 1567–1581. https://doi.org/10.1007/s10570-021-04313-8.

(49) Ogunjobi, J. K.; Balogun, O. M. Isolation, Modification and Characterisation of Cellulose from Wild Dioscorea Bulbifera. *Sci Rep* **2021**, *11* (1), 1025. https://doi.org/10.1038/s41598-020-78533-6.

(50) Thulluri, C.; Balasubramaniam, R.; Velankar, H. R. Generation of Highly Amenable Cellulose-Iβ via Selective Delignification of Rice Straw Using a Reusable Cyclic Ether-Assisted Deep Eutectic Solvent System. *Sci Rep* **2021**, *11* (1), 1591. https://doi.org/10.1038/s41598-020-80719-x.

(51) Kono, H.; Tsukamoto, E.; Tajima, K. Facile Post-Carboxymethylation of Cellulose Nanofiber Surfaces for Enhanced Water Dispersibility. *ACS Omega* **2021**, *6* (49), 34107–34114. https://doi.org/10.1021/acsomega.1c05603.

View Article Online
DOI: 10.1039/D5FB00355E

(52) Rol, F.; Sillard, C.; Bardet, M.; Yarava, J. R.; Emsley, L.; Gablin, C.; Léonard, D.; Belgacem, N.; Bras, J. Cellulose Phosphorylation Comparison and Analysis of Phosphorate Position on Cellulose Fibers. *Carbohydrate Polymers* **2020**, *229*, 115294. https://doi.org/10.1016/j.carbpol.2019.115294.

(53) Chen, S.; Ren, N.; Cui, M.; Huang, R.; Qi, W.; He, Z.; Su, R. Heat Soaking Pretreatment for Greener Production of Phosphorylated Cellulose Nanofibrils with Higher Charge Density. *ACS Sustainable Chem. Eng.* **2022**, *10* (27), 8876–8884. https://doi.org/10.1021/acssuschemeng.2c01904.

(54) Ablouh, E.-H.; Brouillette, F.; Taourirte, M.; Sehaqui, H.; Achaby, M. E.; Belfkira, A. A Highly Efficient Chemical Approach to Producing Green Phosphorylated Cellulosic Macromolecules. *RSC Advances* **2021**, *11* (39), 24206–24216. https://doi.org/10.1039/D1RA02713A.

(55) Ablouh, E.-H.; Kassab, Z.; Hassani, F. S. A.; Achaby, M. E.; Sehaqui, H. Phosphorylated Cellulose Paper as Highly Efficient Adsorbent for Cadmium Heavy Metal Ion Removal in Aqueous Solutions. *RSC Advances* **2022**, *12* (2), 1084–1094. https://doi.org/10.1039/D1RA08060A.

(56) Hou, G.; Zhao, S.; Li, Y.; Fang, Z.; Isogai, A. Mechanically Robust, Flame-Retardant Phosphorylated Cellulose Films with Tunable Optical Properties for Light Management in LEDs. *Carbohydrate Polymers* **2022**, *298*, 120129. https://doi.org/10.1016/j.carbpol.2022.120129.

(57) Rai, R.; Ranjan, R.; Kant, C.; Dhar, P. Biodegradable, Eco-Friendly, and Hydrophobic Drinking Straws Based on Delignified Phosphorylated Bamboo-Gelatin Composites. Rochester, NY March 20, 2023. https://doi.org/10.2139/ssrn.4393891.

(58) Yaradoddi, J. S.; Banapurmath, N. R.; Ganachari, S. V.; Soudagar, M. E. M.; Mubarak, N. M.; Hallad, S.; Hugar, S.; Fayaz, H. Biodegradable Carboxymethyl Cellulose Based Material for Sustainable Packaging Application. *Sci Rep* **2020**, *10* (1), 21960. https://doi.org/10.1038/s41598-020-78912-z.

(59) Liu, M.; Tong, S.; Tong, Z.; Guan, Y.; Sun, Y. A Strong, Biodegradable and Transparent Cellulose-based Bioplastic Stemmed from Waste Paper. *J of Applied Polymer Sci* **2023**, *140* (13), e53671. https://doi.org/10.1002/app.53671.

(60) Nadeem, H.; Dehghani, M.; Garnier, G.; Batchelor, W. Life Cycle Assessment of Cellulose Nanofibril Films via Spray Deposition and Vacuum Filtration Pathways for Small Scale Production. *Journal of Cleaner Production* **2022**, *342*, 130890. https://doi.org/10.1016/j.jclepro.2022.130890.

View Article Online
DOI: 10.1039/D5FB00355E

Data Availability Statement

The information supporting this article has been incorporated within the manuscript. Additional details may be obtained from the corresponding author on request.